Rossby Wave Propagation on a Realistic Longitudinally Varying Flow

BRIAN J. HOSKINS AND TERCIO AMBRIZZI

Department of Meteorology, University of Reading, Whiteknights, Reading, England

(Manuscript received 26 March 1992, in final form 12 August 1992)

ABSTRACT

The response of a barotropic model, linearized about a climatological 300-mb December–February time-mean flow to localized forcing, is considered. In order to aid the design of the experiments and interpretation of the results, a simplified analysis is made of the basic flow in terms of zonal wind, meridional vorticity gradient, and stationary wavenumber. From the analysis the possible existence of a strong waveguide in the Asian jet and weaker waveguides in the North Atlantic and Southern Hemisphere jets is deduced. The possibility of propagation into the equatorial east Pacific and Atlantic oceans and even across these regions is also suggested. These features are confirmed by barotropic model integrations for a variety of perturbation vorticity source positions and shapes. These integrations also show preferred propagation regions arching across North America, from Europe to the Arabian Gulf and, in the Southern Hemisphere, into the equatorial Indian Ocean and Indonesian regions. They also show a tendency to produce a low-wavenumber, fast westward-moving "tail" along the Asian jet. Many of the features found in this study are remarkably consistent with observational teleconnection studies.

1. Introduction

Many previous studies have shown that the barotropic vorticity equation on a sphere, linearized about an upper tropospheric zonal flow, can yield quite realistic tropospheric stationary wave patterns (e.g., Grose and Hoskins 1979; Held 1983). The environment through which a locally excited wave train must propagate in the atmosphere, however, contains marked zonal asymmetries. Thus, the applicability of the research with symmetric basic states to perturbations from a seasonal mean is in some doubt. Following earlier studies by Simmons (1982), Webster and Holton (1982), and Branstator (1983), the investigation described in this paper has been undertaken in order to determine the impact of longitudinal basic-state variations present in the December, January, and February (DJF) time-mean flow on Rossby wave propagation. Baroclinic models have tended to confirm the value of barotropic calculations applied at 300 mb in such investigations (Hoskins and Karoly 1981; Hoskins and Jin 1991).

The earlier studies of teleconnections based on statistics, such as one-point correlation maps, have provided empirical evidence of the existence of recurrent low-frequency patterns in the troposphere. Most of these studies (e.g., Wallace and Gutzler 1981; Blackmon et al. 1984) were based on geopotential height in the Northern Hemisphere. The increasing availability of global data generated at the major weather forecast centers has created the possibility of seeking teleconnections patterns that involve also the subtropics, tropics, and Southern Hemisphere. In their analyses of one-point correlation maps using a 250-mb streamfunction, Hsu and Lin (1992) have attempted to document the major teleconnection patterns and their time evolution (through lag correlation statistics) in a global domain. From their results two more teleconnections regions, apart from those already documented, were found. One such pattern is in the Southern Hemisphere (see their Fig. 11) and another is illustrated by the figure reproduced here as Fig. 1. The lag correlation maps for the base point 25°N, 25°E in Fig. 1 show a wavelike structure that seemingly develops downstream from wave activity in the North American, North Atlantic, and European sectors and propagates downstream along a route skirting the southern Eurasian continent. It then propagates along an arclike route in the North Pacific. Kiladis and Weickmann (1992), through lagged cross correlations between outgoing longwave radiation (OLR) and 200-mb streamfunction, have shown similar results (see their Fig. 8). The case study of Hsu et al. (1990) for the 1985/86 winter intraseasonal oscillation also exhibits similar behavior. One of the major purposes of the present work is to determine whether some of the observed teleconnection patterns can be simulated by subjecting a global barotropic model, linearized about the climatological mean wintertime basic state, to a local forcing. The pattern

Corresponding author address: Dr. Brian J. Hoskins, Department of Meteorology, University of Reading, 2 Early Gate, Whiteknights, P.O. Box 239, Reading, RG6 2AU England.

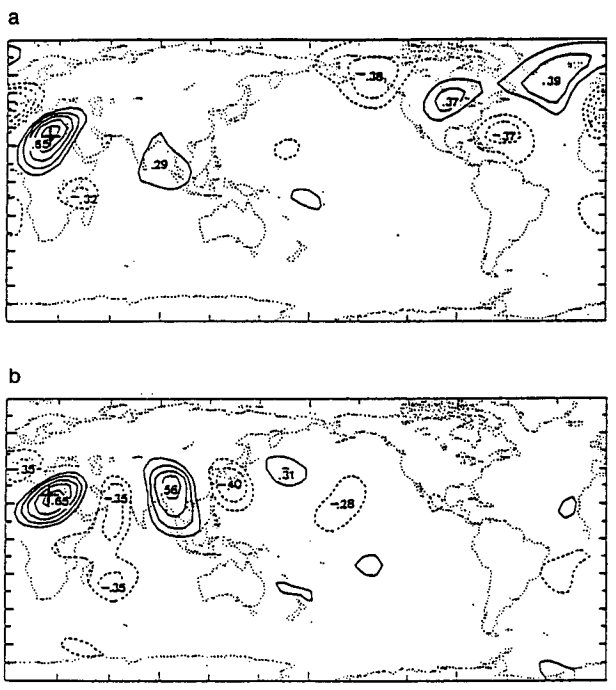

FIG. 1. The lag-correlation between the streamfunction at 25°N, 25°E and the streamfunction at every point (a) 3 days earlier and (b) 3 days later. The contour interval is 0.1, and contours at negative values are dashed. (After Hsu and Lin 1992.)

described above, for instance, is indeed well simulated by the model (see Fig. 4).

In the next section some basic Rossby wave theory will be given and the December–February 300-mb flow is discussed in the light of this theory. Some details of the model are given in section 3. In section 4, an overview of the experiments performed will be presented. Westward propagation, associated with small zonal wavenumbers, in the region of the Asian jet is discussed briefly in section 5. Finally, section 6 highlights the main results of the paper.

2. Theoretical preliminaries

Despite the probable violation of the condition for the strict validity of the theory, many of the model results to be presented in this paper may be understood, at least qualitatively, in terms of the theory of Rossby wave propagation. A review of this theory is given here.

The dispersion relation for barotropic Rossby plane-wave perturbations of the form $\exp[i(kx + ly - \omega t)]$ to a westerly flow, $\bar{U}$, is

$$\omega = \bar{U}k - \frac{\beta_* k}{K^2}, \tag{2.1}$$

where

$$\beta_* = \beta - \frac{\partial^2 \bar{U}}{\partial y^2} \tag{2.2}$$

is the meridional gradient of absolute vorticity and $K = (k^2 + l^2)^{1/2}$ is the total wavenumber. The vector group velocity is

$$\mathbf{c}_g = (u_g, v_g) = \left(\frac{\partial \omega}{\partial k}, \frac{\partial \omega}{\partial l}\right) = (c, 0) + \left(\frac{2\beta_*}{K^2}\right)\cos\alpha \hat{K}, \tag{2.3}$$

where $c = \omega/k$ is the eastward phase speed, $\hat{K}$ is the unit vector normal to the wave crests and troughs with a positive eastward component, and α is the angle this vector makes with the eastward direction.

Stationary Rossby waves ($\omega = 0$, $c = 0$), with

$$K = K_s = \left(\frac{\beta_*}{\bar{U}}\right)^{1/2}, \tag{2.4}$$

are possible if the flow is westerly ($\bar{U}$ positive) and β_* is positive. From (2.3) and (2.4),

$$\mathbf{c}_g = c_g \hat{K}, \tag{2.5}$$

where

$$c_g = 2\bar{U}\cos\alpha. \tag{2.6}$$

The wave activity propagates normal to the crests and troughs with speed $2\bar{U}\cos\alpha$. In particular, stationary Rossby wave activity propagates zonally at twice the flow speed.

As discussed in Hoskins and Karoly (1981, hereafter referred to as HK) and Held (1983), when the basic flow varies slowly in latitude compared with the scale of the waves, the same equations are valid for almost-plane wave solutions. According to this WKB theory, for such a medium that is dependent on y only, as a wave propagates its x wavenumber, k, will be constant, but its y wavenumber, l, will vary such that the local dispersion relation is satisfied. For stationary Rossby waves this implies

$$k = \text{const},$$
$$k^2 + l^2 = K_s^2, \tag{2.7}$$

and the local group velocity is still $c_g = 2\bar{U}\cos\alpha$ in the direction $\hat{K}$.

If α is the angle made by $\hat{K}$ with the x axis,

$$\tan\alpha = \frac{l}{k}. \tag{2.8}$$

Rossby ray paths are refracted in a manner similar to that described by Snell's law in optics. Moving with the group velocity, $\mathbf{c}_g$, from (2.7) the rates of changes of k and l are given by

$$\frac{d_g k}{dt} = 0$$

$$\frac{d_g l}{dt} = \frac{K_s}{l}\frac{d_g K_s}{dt} = \frac{K_s}{l} v_g \frac{dK_s}{dy},$$

but, from (2.5), $v_g/l = c_g/K_s$, and so

$$\frac{d_g l}{dt} = c_g \frac{dK_s}{dy}. \tag{2.9}$$

From (2.8), the bending of the ray is given by

$$\frac{d_g}{dt}\tan\alpha = \frac{1}{k} c_g \frac{dK_s}{dy}, \tag{2.10a}$$

or

$$\frac{d_g \alpha}{dt} = \frac{k}{K_s^2} c_g \frac{dK_s}{dy}. \tag{2.10b}$$

Therefore, Rossby rays are always refracted toward latitudes with larger K_s. Defining the radius of curvature of the ray path, r, to be positive if it is bending in an anticlockwise manner,

$$\frac{d_g \alpha}{dt} = \frac{c_g}{r},$$

and so the ray path radius of curvature is given by the simple expression

$$r = K_s^2 \Big/ \left(k \frac{dK_s}{dy}\right) \tag{2.11a}$$

or

$$r^{-1} = -k \frac{dK_s^{-1}}{dy}. \tag{2.11b}$$

The curvature is clockwise if K_s increases toward the equator and anticlockwise if it increases toward the pole. The curvature is large if K_s^{-1} changes rapidly. Although the notion of Rossby wave refraction has been frequently discussed, (2.10) and (2.11) do not appear to have been published previously. Similar results, but for latitudinal–vertical Rossby wave propagation in a flow varying in both these directions, have been given in Karoly and Hoskins [1982, Eqs. (27) and (28)].

It is useful to consider the schematic situations given in Fig. 2. Figure 2a shows the refraction toward higher values of K_s. Figure 2b shows a ray reflected from a turning latitude, Y_{TL}, at which $K_s = k$ and $l = 0$. Extensions of the theory predict decay beyond this latitude. Figure 2c includes a latitude, Y_B, at which β_*, and hence K_s, is zero. All rays must turn before this latitude. Figure 2d includes a critical latitude, Y_{CL}, at which $\bar{U}$ is zero and K_s becomes infinite. Rays are refracted normally into such a line but with the meridional scale and group velocity tending to zero. The theory is not valid very close to the critical line and study of such regions by Killworth and McIntyre (1985, and references therein) has suggested that they can become reflecting regions when nonlinearity is fully taken account of. Finally, Fig. 2e shows a local maximum in K_s. Waves with zonal wavenumber in the range $K1$ and $K2$ are trapped, and such a K_s maximum provides

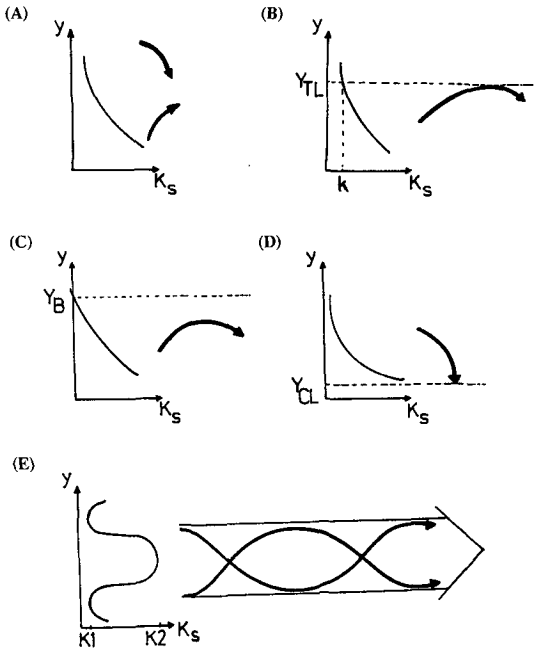

FIG. 2. Schematic stationary Rossby wavenumber (K_s) profiles and ray path refraction. In each panel, K_s is shown as a function of y and schematic ray paths are shown by heavy lines with arrowheads. (a) simple refraction; (b) reflection from a turning latitude Y_{TL} at which $K_s = k$; (c) reflection of all wavenumbers before a latitude Y_B at which $\beta_* = 0$; (d) refraction into a critical latitude Y_{CL} at which $\bar{U} = 0$; (e) waveguide effect of a K_s maximum. For more discussion see text.

a Rossby waveguide. This situation is particularly likely to occur in a strong westerly jet. Because of the curvature of the flow, β_* tends to have a larger relative maximum than does $\bar{U}$. Consequently, strong westerly jets can act as Rossby waveguides.

The strict validity of WKB theory for Rossby wave propagation on realistic flows is questionable. Indeed, in the strong jet waveguide case, the scale of the waves K_s^{-1} and the scale of the basic flow are both $(\bar{U}/|\bar{U}_{yy}|)^{1/2}$ (I. M. Held, personal communication). It has been found in HK that the theory is qualitatively useful even in such situations where the WKB small number approaches unity.

In HK it was also shown that the effects of spherical geometry can be included in the WKB treatment. As shown in section 5b of that paper, the Mercator coordinate equivalent of the poleward absolute vorticity gradient, β_*, is

$$\beta_M = \left[2\Omega - \left(\frac{1}{\cos\phi}\frac{\partial}{\partial\phi}\right)^2 (\cos^2\phi \bar{v})\right] \frac{\cos^2\phi}{a}, \tag{2.12}$$

where ϕ is the latitude and $\bar{v} = \bar{U}/a\cos\phi$ is the relative rotation rate of the atmosphere; β_M is $\cos\phi$ times the meridional gradient of absolute vorticity on the sphere. The stationary wavenumber may be written in terms

of an equivalent zonal wavenumber on the Mercator projection:

$$K_s = \left(\frac{a\beta_M}{\bar{v}}\right)^{1/2} = \left\{\left[2\Omega - \left(\frac{1}{\cos\phi}\frac{\partial}{\partial\phi}\right)^2(\cos^2\phi\bar{v})\right]\Big/\bar{v}\right\}^{1/2}\cos\phi. \quad (2.13)$$

Karoly (1983) has extended ray theory to the case of a basic flow ($\bar{U}$, $\bar{V}$) with longitudinal as well as latitudinal variation. The ray equations contain the flow and its first derivatives, and the absolute vorticity and all its first and second derivatives. Their complexity is such that numerical solution is necessary and little direct insight is possible. Given the dominance in large-scale flow fields of $\bar{U}$ over $\bar{V}$, and latitudinal over longitudinal gradients of the basic flow, it seems probable that most of the useful results from ray theory can be obtained by consideration of the quantities $\bar{U}$, β_*, and K_s. For example, from Karoly [1983, Eq. (8)], for stationary waves

$$K^2 = \frac{\partial\bar{\zeta}/\partial y - (l/k)\partial\bar{\zeta}/\partial x}{\bar{U} + (l/k)\bar{V}},$$

where $\bar{\zeta}$ is the basic flow absolute vorticity. If ϵ is a measure of the anisotropy of the basic flow, that is, $\bar{V}/\bar{U}$ and $(\partial\bar{\zeta}/\partial x)/(\partial\bar{\zeta}/\partial y)$ are both of order ϵ, then

$$K^2 = K_s^2 + O(\epsilon\tan\alpha),$$

where $K_s^2(x, y)$ is defined as in (2.4) but using local values. Similarly, to first order in ϵ, $\mathbf{c}_g$ is given by (2.5) and (2.6) using the local $\bar{U}$, and the changes in k along a ray path may be neglected compared with those in l. Thus, we shall apply the theory of (2.1) to (2.13) locally. This extra approximation is particularly worthwhile because basic flow variations occur on such a short meridional scale that ray theory can only be used for qualitative argument.

Most previous barotropic studies have used 300-mb basic flows, and this will be done here also although, as will be discussed below, sensitivity studies have been performed with flows from other levels. Equivalent barotropic, midlatitude structures are probably best represented using the flow from a slightly lower level (Held et al. 1985). From HK, however, it appears that it is the upper tropospheric winds that are relevant for Rossby wave propagation in the tropical and subtropical regions. The 300-mb level is then a compromise between these two choices.

The basic flow used in this paper is a six-year, 1979–85, December–February time-mean 300-mb rotational flow derived from the European Centre for Medium-Range Weather Forecasts (ECMWF) analyses. Various aspects of this flow are shown in Fig. 3, all of which tend to emphasize the existence of large length-scale variations in the longitudinal direction as well as shorter length-scale variations in latitude. They therefore suggest that local propagation characteristics can be expected to deviate significantly from those detailed by HK for the zonally averaged flow but that the local application of the above ray theory for a flow depending on latitude only may indeed be qualitatively useful.

The zonal wind (Fig. 3a) shows the Asian, North American, and Southern Hemisphere extended maxima. There are significant easterlies equatorward of the Asian jet maximum, but there are westerlies in the equatorial east Pacific and also in the Atlantic. The absence of a zero wind line in these regions has led a number of authors—for example, Webster and Holton (1982)—to suggest that they may be favorable regions for cross-equatorial propagation.

The jet regions do indeed exhibit strong maxima in the meridional absolute vorticity gradient, β_M, shown in Fig. 3b, with minima to the north and south of the jets. For the strong Asian jet, the minima are close to zero or even negative. The magnitudes of, and variations in, β_M are striking compared with the planetary term alone, which would vary smoothly from 2.3 in these units to zero at the poles.

Figure 3c gives the geographical distribution of K_s, defined by (2.13), for β_M and $\bar{U}$ positive. The zero wind line, $\bar{U} = 0$, is shown by a thickened contour and the zero β_M and K_s (but positive $\bar{U}$) line by dots. Each jet region contains quite uniform values of K_s bounded meridionally by lower values.

From the Rossby wave theory described above and Fig. 3c (and Figs. 3a,b), the possibility of the following properties for Rossby wave propagation is suggested:

1) a strong waveguide along the Asian jet from North Africa to the western North Pacific, with typical stationary wavenumber 7;

2) a waveguide along the North Atlantic jet from the western North Atlantic to northern Europe, with typical stationary wavenumber 5;

3) a waveguide in the region of the Southern Hemisphere jet, with typical stationary wavenumber 5–6; and

4) wave propagation regions into the equatorial east Pacific and Atlantic oceans with some possibility of very weak cross-equatorial propagation.

Numerical integrations of a barotropic model designed to test the existence of such features or other propagation characteristics will now be described.

3. The barotropic model

The basic model used in this study is based on the damped barotropic vorticity equation

$$\left(\frac{\partial}{\partial t} + \mathbf{V}_\Psi\cdot\nabla\right)\zeta = F - \lambda\zeta - \mu\nabla^4\zeta, \quad (3.1)$$

where $F = \bar{F} + F'$ is a constant forcing, λ is a linear damping with a time scale of 10 days, and $\mu = 2.338\ 10^{16}\ \mathrm{m^4\ s^{-1}}$. The equation is solved using the spectral

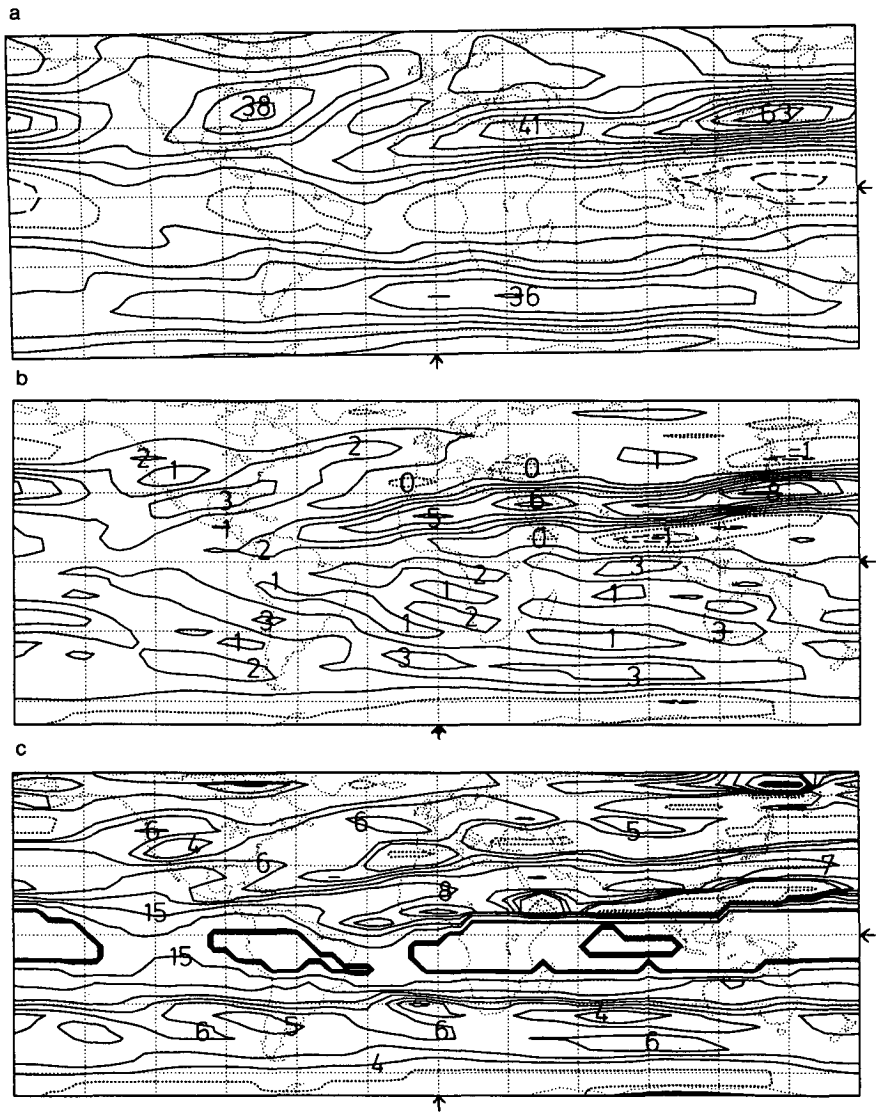

FIG. 3. The climatological DJF 300-mb flow based on ECMWF data for the period 1979–85. (a) Westerly component of the wind, U; contour interval 6 m s^{-1}. (b) Mercator coordinate meridional gradient of the absolute vorticity, β_M, defined in (2.12); contour interval 1.10^{-11} s^{-1} m^{-1}. (c) Stationary wavenumber, K_s, defined in (2.13) for β_M and $\bar{U}$ positive; contours at zonal wavenumbers 0, 4, 5, 6, 7, 8, 10, and 15, and also 25–30, producing a thickened contour indicating singular values of K_s. In all panels, negative contours are dashed and zero contours are dotted. Lines of latitude and longitude are drawn every 30°, and arrows indicate 0° latitude and longitude.

transform technique with a triangular truncation at wavenumber 21, the biharmonic diffusion acting on a time scale of about 4 days on the smallest length scale.

The forcing $\bar{F}$ is determined such that the basic state used is an exact solution of (3.1). The perturbation forcing F' is intended purely as a local source of Rossby waves and is specified as fD, where f is the Coriolis parameter and the divergence D, in general, has a cosine squared amplitude in an ellipse with semiaxis 45° in longitude and 22.5° in latitude or a circle of radius 30°. Consequently, the perturbation vorticity forcing takes the form of a dipole when it is centered on the equator, but a monopole when it is away from the equator. The magnitude of the vorticity forcing is small near the equator. The actual structure of F' for the various solutions discussed in section 4 is shown in Fig. 4. In most experiments D is multiplied by 10^{-6} so that the calculation is effectively linear but the results are scaled so that the maximum value of D is equal to 3×10^{-6} s^{-1}, which according to HK, corresponds to the outflow associated with about 5 mm day^{-1} of tropical precipitation.

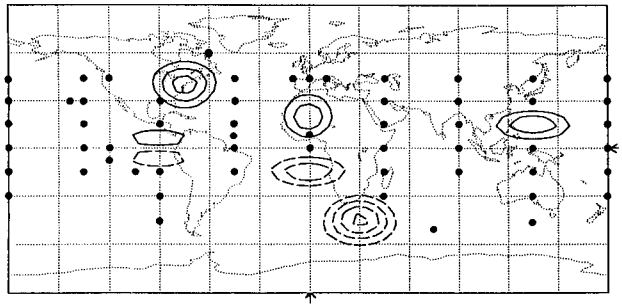

FIG. 4. Perturbation forcings. The dots indicate the centers of the forcings used in the range of experiments performed. The structure of F' used in various solutions discussed in the paper is shown by contours. The contouring is such as to show the vorticity that F' would generate in 1½ days [2½ days for the (0°, 90°W) forcing], with the same contour interval as used in Figs. 5–10.

4. Barotropic results

a. Results presentation

The total range of experiments performed with the barotropic model described in section 3 is summarized in Fig. 4. For some selected points, nonlinear barotropic and linear equivalent barotropic experiments have also been performed. These will be mentioned in the Conclusions section. The experiments to be presented below have been chosen in such a way as to give an overview of the main wave propagation patterns found.

All pictures to be shown are of the relative vorticity perturbation from the initial December–February mean flow. Sometimes the nature of the propagation of wave activity is evident only using fine temporal resolution or detailed contouring of results. Such pictures will in general not be presented but the comments made reflect detailed analysis of them.

b. Model results

1) NORTH AFRICAN–ASIAN JET ENTRANCE

The data study of Hsu and Lin (1992) and the theory in section 2 have suggested that the North African–Asian jet stream may act like a waveguide. To test this, the first experiment uses a circular divergence placed at 20°N, 0°, near the west end of the jet. The solution at days 4, 7, 10, and 15 is shown in Fig. 5. As shown by the day 4 picture, Rossby wave activity does indeed propagate along the Asian jet stream waveguide. It moves at about 50 m s^{-1}, and produces alternate signs in vorticity with a zonal wavelength of about 75° of longitude. The implied zonal wavenumber 5 together with the meridional scale is equivalent to a total wavenumber 7–8. The speed of the wave activity is close to but somewhat less than the theoretical value of twice the ambient zonal wind. The wave scale is close to that given by the theory.

At day 7, the positions of the vorticity maxima and minima are very similar with the downstream propagation continuing into the east Pacific. By day 10 this propagation has curved southeastward into the equatorial east Pacific, with a center even at 20°S. With a

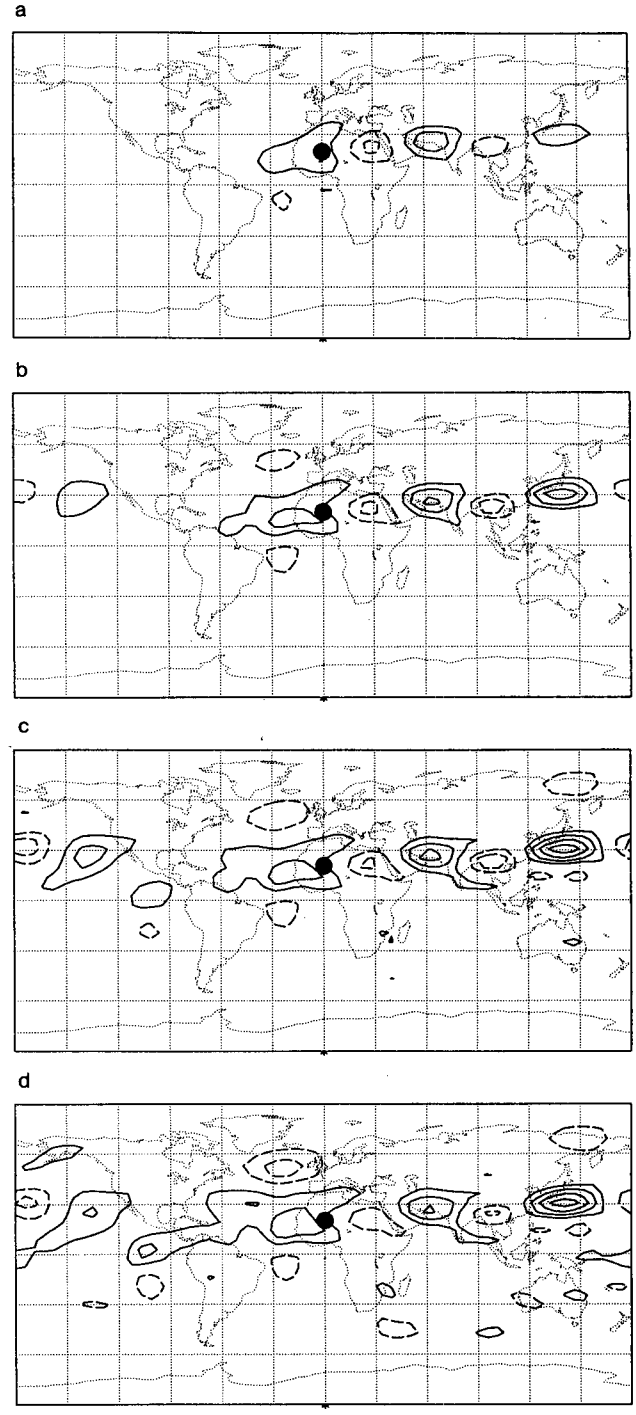

FIG. 5. The model relative vorticity anomaly at (a) day 4, (b) day 7, (c) day 10, and (d) day 15 for a forcing centered at 20°N, 0°. The contour interval is 8×10^{-6} s^{-1}, negative values are dashed, and the zero contour is not shown. The black circle indicates the forcing position.

fine contour interval, it is seen that the propagation path splits in the North Pacific with a weaker train of waves passing over North America. The perturbation near (30°N, 140°E) has continued to grow and has become the largest anomaly.

There is already a marked similarity between the observed patterns shown in Fig. 1b and those found at day 7. The observational studies of Hsu and Lin (1992) and Kiladis and Weickmann (1992) and the theoretical study of Webster and Holton (1982) support the southeastern propagation into the equatorial east Pacific. The large amplitude center near 140°E is found in a number of studies. It occurs close to the maximum of $\bar{U}$ and β_M with negative β_M to the north and south. Branstator (1983) has suggested that an interpretation of this eddy maximum is that wave overreflection by the zero β_M lines is occurring.

The day 15 picture in Fig. 5 gives a hint of wave propagation from the equatorial Atlantic just south of the equator in an arc around the southern Indian Ocean to Australia. This pattern will occur more clearly in an experiment to be discussed below.

The use of a zonally elongated source produces smaller amplitude propagation along the waveguide than seen in Fig. 5. This is entirely consistent with the bias toward meridional propagation suggested by theory for such a source.

It should be noted that even though our initial value technique must generate waves of all frequencies, the vorticity maxima and minima are almost stationary and the comparison with stationary Rossby wave theory is valid.

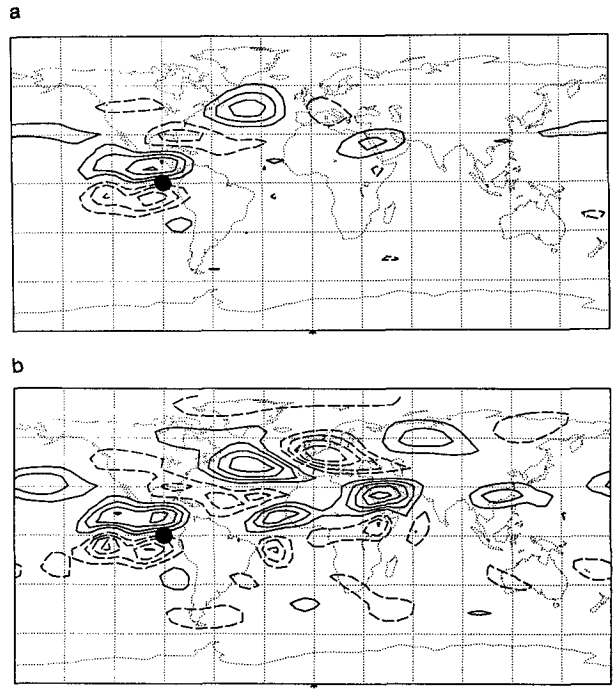

FIG. 6. The model vorticity anomaly for the forcing centered at 0°, 90°W at (a) day 6 and (b) day 12. Contour conventions as in Fig. 5.

2) WEST OF NORTH ATLANTIC JET

Putting an elliptical region of divergence centered at (0°, 90°W) produces a north and northeasterly propagating wave train that enters the North Atlantic jet region, which has been identified as a possible waveguide. At day 6 (Fig. 6a), there is an arching Northern Hemisphere pattern with centers over the southeastern United States and central Atlantic, in the North Atlantic jet, and downstream centers over southern Europe, the Arabian Gulf, and with weak magnitude over Ethiopia. By day 12 (Fig. 6b), a second propagation pattern, from the central North Atlantic across northern Eurasia, is also apparent. These wave trains resemble the "Eurasian" and "Middle East" patterns found in the observational studies by Wallace and Gutzler (1981) and Blackmon et al. (1984). It appears that wave activity is indeed guided by the North Atlantic jet waveguide. The Mediterranean flank of the waveguide is locally weak enough that wave activity can leak across to the Arabian Gulf region. Between the zero values in K_s in Fig. 3c in the western Mediterranean and Middle East, the value reaches more than 4. Otherwise, the wave activity follows the weak guide to 60°N over eastern Asia. The eastward propagation speed from the central North Atlantic between day 6 and day 12 is 20–25 m s^{-1}, which is about double the flow speed. The zonal wavenumber is about 3, which is consistent with a total wavenumber of about 5.

There is a hint of other wave patterns also in Fig. 6. Some wave activity appears to travel on much tighter arcs in both the Northern and Southern hemispheres. There is also some evidence of wave activity propagation across the tip of South America and around the Southern Ocean. Such propagation will be seen more clearly in later examples.

3) IN THE NORTH ATLANTIC JET

With circular forcing at (40°N, 75°W) near the North Atlantic jet stream maximum, the day 12 solution (Fig. 7) shows many of the features seen in the previous solution (Fig. 6). There is the North Atlantic jet guide with its Arabian Gulf leakage as well as its Eurasian extension. The wavelength of the northern pattern is similar but the nodes are shifted by almost a quarter-wavelength. This time the wave path extends across the Pacific before propagating south-southeast into the equatorial eastern Pacific. There is evidence of direct propagation into the equatorial Atlantic.

4) WEST PACIFIC

Many previous studies with barotropic and baroclinic models have used forcing in the tropical west

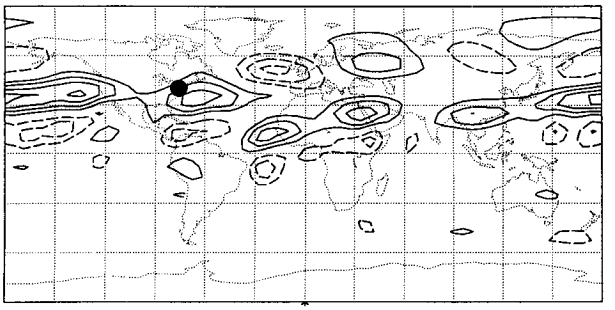

FIG. 7. The model vorticity anomaly at day 12 for the forcing at 40°N, 75°W. Contour conventions as in Fig. 5.

Pacific. For completeness, we show in Fig. 8 the day 12 solution for an elliptical forcing centered just east of the Philippines at 15°N, 135°E. The two elongated centers near 150°E have a very large amplitude, in agreement with the barotropic growth found by Simmons et al. (1983). These centers are part of an arclike pattern across the North Pacific with most of the wave activity propagating into, and partially through, the eastern equatorial Pacific westerlies. Some wave activity, however, propagates across North America. The pattern involving the three centers at 30°N, 150°W; 50°N, 120°W; and in the Florida region are reminiscent of the Pacific/North American (PNA) pattern of Wallace and Gutzler (1981).

5) SOUTHERN HEMISPHERE TROPICAL WESTERLIES

In the previous experiments there were signs of propagation into the Southern Hemisphere in the regions of tropical westerlies in the east Pacific and Atlantic and, in the two cases shown in Fig. 5 and Fig. 6, of wave patterns in this hemisphere emanating from the westerlies regions.

To examine this further, the day 12 results of experiments with elliptical forcing centered at 15°S, 105°W and 15°S, 0° are shown in Fig. 9. The former (Fig. 9a) is similar to that for 0°, 90°W already presented in Fig. 6b. In particular, wave activity propagates across the equator and into the North Atlantic and North African–Asian waveguides, and there is a wave path across South America and into the equatorial Atlantic. There is also a path around the tips of South America and South Africa and into the equatorial Indian Ocean. In retrospect, evidence of such a path can be found in Fig. 6b. A similar wave propagation route in the atmosphere has been suggested by Gao and Stanford (1988), using four years of satellite-derived microwave brightness temperatures. Recent barotropic numerical calculations and observational data analyses for winter and summer for the Southern Hemisphere by Berbery et al. (1992) have shown similar results. In particular, their height teleconnection patterns (Fig. 8f) and the composites of observed streamfunction anomalies for the summer teleconnection patterns (Fig. 11c,d) are in good agreement with the ray paths described above.

The southern equatorial Atlantic forcing (Fig. 9b) also leads to wave activity entering the two Northern Hemisphere waveguides. The wave activity appears to be split by the region of low stationary wavenumber, shown in Fig. 3c, reaching west-southwest from the western Mediterranean. The Southern Hemisphere wave propagation proceeds in an arc to 50°S in the Indian Ocean and crosses Australia. Comparing with Fig. 3c, it is seen that the wave activity closely follows the stationary wavenumber maximum leading from

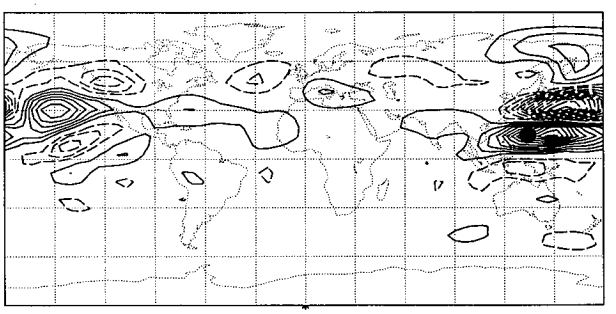

FIG. 8. The model vorticity anomaly at day 12 for the forcing at 15°N, 135°E. Contour conventions as in Fig. 5.

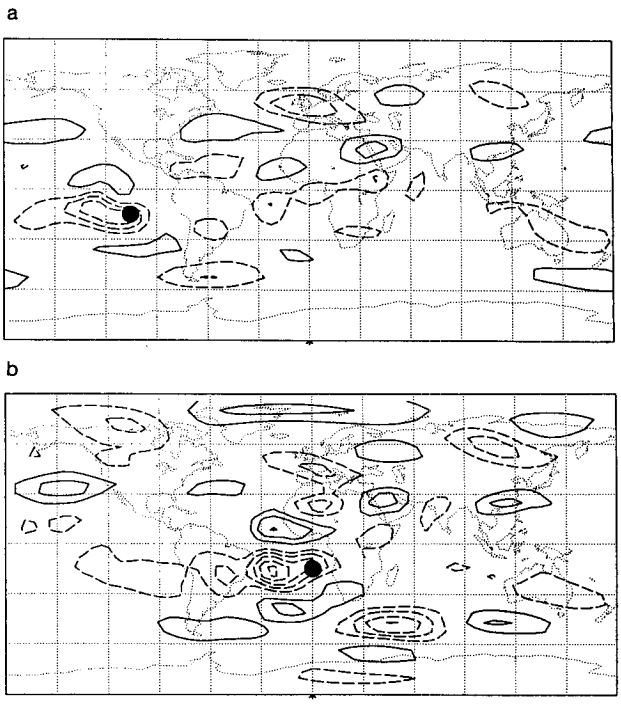

FIG. 9. The model vorticity anomaly at day 12 for the forcing centered at (a) 15°S, 105°W and (b) 15°S, 0°. Contour conventions as in Fig. 5.

40°S, 15°W into the jet waveguide at 50°S in the Indian Ocean and then propagates equatorward, where it weakens. Although Gao and Stanford did not comment on such a pattern, it is perhaps present in their Figs. 1 and 3. Kiladis and Weickmann (1992) also had evidence of such a pattern in their Fig. 6c.

6) SOUTHERN HEMISPHERE JET

To focus on the Southern Hemisphere jet, results are now given for a circular forcing centered in it at 45°S, 30°E. By day 4 (Fig. 10a) one wavelength has been generated along the jet, the wave activity moving at about 35 ms^{-1} and having a zonal wavenumber 3. The speed is between one and two times the basic flow speed in the region and the zonal wavenumber is consistent with the stationary wavenumber of 5–6 in the region. There are signs of a split of the wave activity west of Australia where the waveguide weakens, with some of the activity propagating across Australia in the manner seen in Fig. 9b. By day 12 (Fig. 10b) the two patterns are clearer. The wave train across Australia has the characteristics of propagation toward a critical line as described by HK. The meridional wavelength becomes smaller, the path becomes more meridional, and the propagation speed becomes smaller. The wave train south of Australia arches toward the equatorial east Pacific, with signs of activity propagating also into the South Atlantic. It is clear that, again, activity moves into the Northern Hemisphere, producing the North Atlantic–Eurasian–North Pacific arc and the North African–Asian jet region response.

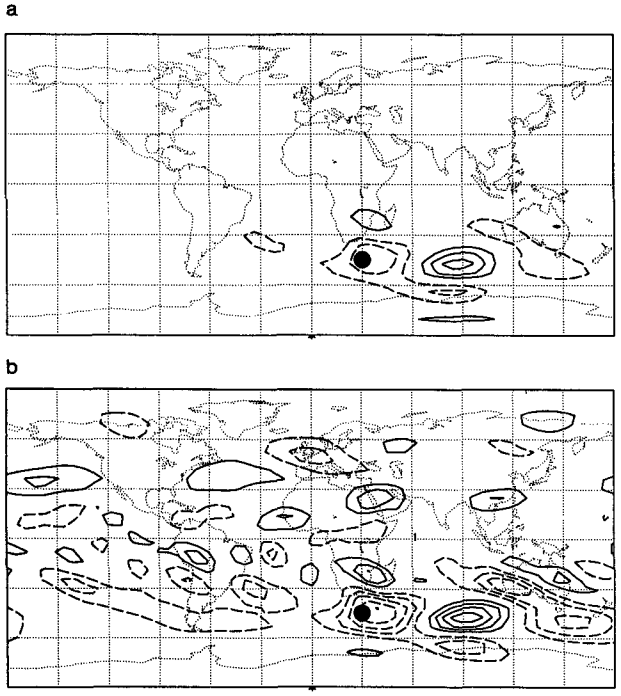

FIG. 10. The model vorticity anomaly for the forcing centered at 45°S, 30°E at (a) day 4 and (b) day 12. Contour conventions as in Fig. 5.

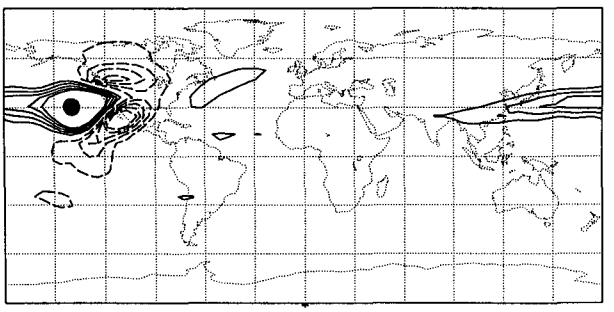

FIG. 11. The model vorticity anomaly at day 1 for the forcing centered at 30°N, 140°W. The contours are plotted only between $\mp 5 \times 10^{-6}$ s^{-1} with an interval of 1×10^{-6} s^{-1}.

The wave propagation pattern in the Southern Hemisphere jet agrees with the numerical results of Berbery et al. (1992). In their observational data analysis, the wave activity flux vectors (Fig. 9b,d) support the idea of propagation of wave activity inside the jet and also show an equatorward orientation in the east of Australia, in good agreement with the wave propagation patterns found in our results.

5. Westward propagation

A number of the integrations performed showed the rapid westward movement of vorticity of one sign, in addition to the eastward development of a wave train. Figure 7 provides an example in which positive vorticity stretches westward from the source region along the Asian jet region, with all the centers having a positive sign. To focus on this feature, Fig. 11 shows the day 1 solution for a circular forcing centered at 30°N, 140°W just east of the strong β_M values associated with the Asian jet. The contouring is modified to emphasize the fringe propagation details. There is a very clear upstream propagation along the β_M maximum. The fringe covers 70°–130° in one day, a speed of 65–125 m s^{-1}.

In the limit of long zonal wavelength, the zonal phase speed and group velocity both become equal to $-\beta_*/l^2$. This implies the development of an upstream "tail," which has been seen in all the barotropic integrations since Hoskins et al. (1977). Here, however, with the very large values of β_* in the Asian jet, it is particularly strong and fast. Taking $\beta_* = 7 \times 10^{-11}$ m^{-1} s^{-1} and a half-wavelength $\pi/l = 3 \times 10^6$ m gives the westward speed to be 64 m s^{-1}, consistent with the model results.

A more physical view can be obtained by considering the situation shown in Fig. 12. A positive vorticity anomaly in the Northern Hemisphere induces a cyclonic circulation. On the eastern side, this flow brings low vorticity air from the south and produces a negative vorticity anomaly. In this manner the downstream wave pattern is produced. On the western side, how-

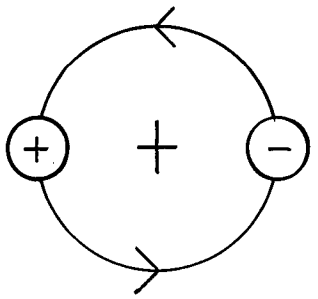

FIG. 12. An idealized picture showing a Northern Hemisphere positive vorticity anomaly (indicated by a +) with its induced cyclonic circulation. The vorticity tendencies implied by the meridional advection by this circulation are shown by the circled signs.

ever, high vorticity air from the north is advected in, producing a vorticity anomaly of the same sign as the original. For a wave with alternating signs in vorticity, such a generation corresponds simply to the westward movement of the Rossby wave relative to the flow. For an isolated vorticity extremum the induced circulation is markedly broader than the forcing anomaly and the generation corresponds to an upstream extension of that anomaly. This mechanism is particularly effective where the meridional vorticity gradient, β_*, is large, as it is in the Asian jet.

6. Discussion

The results of all the linear barotropic experiments performed using the December–February 300-mb flow, some of which have been described here, are summarized in Fig. 13. The background contours are some of the key ones from the basic flow stationary wave figure (Fig. 3c). The three waveguides, the North African–Asian jet, the North Atlantic jet–North European region, and the Southern Hemisphere jet, are shown by arrows with cross-hatched shafts. The preferred propagation toward and away from these waveguides is indicated by single-shafted arrows. The westerly regions in the tropical east Pacific and Atlantic play an important role here. The other propagation patterns are from Europe through the Arabian Gulf and across North America in the Northern Hemisphere, and into the tropical Indian Ocean and west Pacific in the Southern Hemisphere.

It has been suggested (I. M. Held, personal communication) that an alternative, and indeed opposite perspective of the waveguide nature of jets to that given by slowly varying WKB theory, is to consider them as discontinuities in vorticity. For a zonally oriented "vorticity front" there is no meridional propagation, and waves propagate zonally with phase speed $c = \bar{U} - \Delta/k$, where Δ is the vorticity jump across the jet. In this case the zonal group velocity is $\bar{U}$ rather than twice this. It appears that this alternative view is useful for the very strong North African–Asian jet. It was commented in section 4b that the speed of propagation of wave activity is indeed less than twice the local zonal wind speed.

A number of experiments have been repeated with linear barotropic models applied to the 150-mb flow, and with nonlinear barotropic and linear equivalent barotropic models applied to the 300-mb flow. The differences found are generally quantitative rather than qualitative, and the summary in Fig. 13 appears to be quite robust. The role of the tropical westerly regions and evidence for cross-equatorial propagation are enhanced at the 150-mb level. Baroclinic model results, to be reported elsewhere, also generally support this picture. The westward propagation along the Asian jet is significantly reduced, though still present.

One of the basic assumptions in the modeling described here is that the basic state is maintained by a forcing $\bar{F}$ that does not vary as the flow varies. Andrews (1984) showed that if the basic flow was maintained by orographic forcing, it can be stable or unstable depending on which orography is chosen. As a partial test of the sensitivity of our results to the assumption

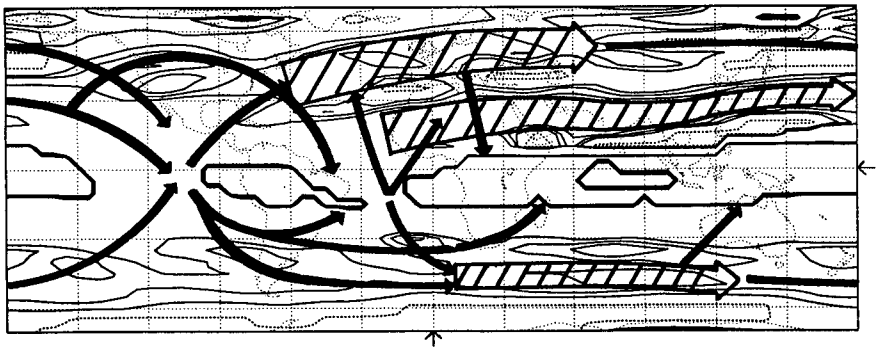

FIG. 13. A schematic summary of the waveguides shown by the cross-hatched shafted arrows, and the preferred propagation patterns, indicated by the single-shafted arrows, deduced from the range of experiments depicted in Fig. 4. The background contours are those for K_s equal to 0, 4, 5, 6, and 25–30 taken from Fig. 3c.

of constant $\bar{F}$, an experiment was performed in which the form chosen for $\bar{F}$ was that suggested by the study of Sardeshmukh and Hoskins (1988):

$$\bar{F} = -\nabla \cdot (\bar{v}_\chi \zeta) + \bar{\bar{F}}.$$

Here $\bar{v}_\chi$ was determined by solving the χ problem (Sardeshmukh and Hoskins 1987) and $\bar{\bar{F}}$ is a constant forcing that makes the basic-state solution exact. As the vorticity changes, $\bar{F}$ changes; however, there was found to be little qualitative change in wave propagation in the 12-day period of interest here.

In general, results from the simple model used here agree remarkably well with observations, and in particular these of Hsu and Lin (1992), Kiladis and Weickmann (1992), and, in the Southern Hemisphere, Gao and Stanford (1988) and Berbery et al. (1992). The fact that simple wave propagation ideas provide a qualitative and even quantitative interpretation of the results, even though the strict mathematical validity for the application of the theory is in doubt, gives a very useful theoretical basis for discussion of teleconnection behavior in the atmosphere.

Acknowledgments. We wish to acknowledge very useful comments made by G. Branstator, I. Held, D. Stephenson, J. Thuburn, and anonymous reviewers on an early version of this paper. One of us (TA) wishes to acknowledge CNPq (Conselho Nacional de Desenvolvimento Científico e Tecnológico), responsible for the financial grant support, and IAG-USP (Instituto Astrônomico e Geofísico, Universidade de São Paulo), in Brazil, which allowed the completion of this research.

REFERENCES

Andrews, D. G., 1984: On the stability of forced non zonal flow. *Quart. J. Roy. Meteor. Soc.*, **110,** 657–662.

Berbery, E. H., J. Nogués-Paegle, and J. D. Horel, 1992: Wavelike Southern Hemisphere extratropical teleconnections. *J. Atmos. Sci.*, **49,** 155–177.

Blackmon, M. L., Y.-H. Lee, and J. M. Wallace, 1984: Horizontal structure of 500 mb height fluctuations with long, intermediate and short time scales. *J. Atmos. Sci.*, **41,** 961–979.

Branstator, G. W., 1983: Horizontal energy propagation in a barotropic atmosphere with meridional and zonal structure. *J. Atmos. Sci.*, **40,** 1689–1708.

Gao, X. H., and J. L. Stanford, 1988: Possible feedback path for low-frequency atmospheric oscillations. *J. Atmos. Sci.*, **45,** 1425–1432.

Grose, W. L., and B. J. Hoskins, 1979: On the influence of orography on large scale atmospheric flow. *J. Atmos. Sci.*, **36,** 223–234.

Held, I. M., 1983: Stationary and quasi-stationary eddies in the extratropical troposphere: Theory. *Large-Scale Dynamical Processes in the Atmosphere,* B. J. Hoskins and R. P. Pearce, Eds., Academic Press, 127–168.

——, R. L. Panetta, and R. T. Pierrehumbert, 1985: Stationary external Rossby waves in vertical shear. *J. Atmos. Sci.*, **42,** 865–883.

Hoskins, B. J., and D. J. Karoly, 1981: The steady linear response of a spherical atmosphere to thermal and orographic forcing. *J. Atmos. Sci.*, **38,** 1179–1196.

——, and F.-F. Jin, 1991: The initial value problem for tropical pertubations to a baroclinic atmosphere. *Quart. J. Roy. Meteor. Soc.*, **117,** 299–317.

——, A. J. Simmons, and D. G. Andrews, 1977: Energy dispersion in a barotropic atmosphere. *Quart. J. Roy. Meteor. Soc.*, **103,** 553–567.

Hsu, H.-H., and S.-H. Lin, 1992: Global teleconnections in the 250-mb streamfunction field during the Northern Hemisphere winter. *Mon. Wea. Rev.*, **120,** 1169–1190.

——, and B. J. Hoskins, and F.-F. Jin, 1990: The 1985/86 intraseasonal oscillation and the role of the extratropics. *J. Atmos. Sci.*, **47,** 823–839.

Karoly, D. J., 1983: Rossby wave propagation in a barotropic atmosphere. *Dyn. Atmos. Oceans,* **7,** 111–125.

——, and B. J. Hoskins, 1982: Three dimensional propagation of planetary waves. *J. Meteor. Soc. Japan,* **60,** 109–123.

Kiladis, G. N., and K. M. Weickmann, 1992: Circulation anomalies associated with tropical convection during northern winter. *Mon. Wea. Rev.*, **120,** 1900–1923.

Killworth, P. D., and M. E. McIntyre, 1985: Do Rossby wave critical layers absorb, reflect, or over-reflect? *J. Fluid Mech.*, **161,** 449–492.

Sardeshmukh, P. D., and B. J. Hoskins, 1987: On the derivation of the divergent flow from the rotational flow: The Chi-problem. *Quart. J. Roy. Meteor. Soc.*, **113,** 339–360.

——, and ——, 1988: The generation of global rotational flow by steady idealized tropical divergence. *J. Atmos. Sci.*, **45,** 1228–1251.

Simmons, A. J., 1982: The forcing of stationary wave motion by tropical diabatic heating. *Quart. J. Roy. Meteor. Soc.*, **108,** 503–534.

——, J. M. Wallace, and G. W. Branstator, 1983: Barotropic wave propagation and instability, and atmospheric teleconnection patterns. *J. Atmos. Sci.*, **40,** 1363–1392.

Wallace, J. M., and D. S. Gutzler, 1981: Teleconnections in the geopotential height field during the Northern Hemisphere winter. *Mon. Wea. Rev.*, **109,** 785–812.

Webster, P. J., and J. R. Holton, 1982: Cross-equatorial response to middle latitude forcing in zonally varying basic state. *J. Atmos. Sci.*, **39,** 722–733.